Large surface conductance and superconductivity in topological insulator microstructures

Yangmu Li (iD), Jie Wu, Fernando Camino, G. D. Gu, Ivan Božović, and John M. Tranquada (iD)

ARTICLES YOU MAY BE INTERESTED IN

Large surface conductance and superconductivity in topological insulator microstructures

Yangmu Li,[1,a] (iD) Jie Wu,[1] Fernando Camino,[2] G. D. Gu,[1] Ivan Božović,[1] and John M. Tranquada[1] (iD)

AFFILIATIONS

[1]Condensed Matter Physics and Materials Science Division, Brookhaven National Laboratory, Upton, New York 11973, USA
[2]Center for Functional Nanomaterials, Brookhaven National Laboratory, Upton, New York 11973, USA

[a]Author to whom correspondence should be addressed: yangmuli@bnl.gov

ABSTRACT

Controllable geometric manipulation via micromachining techniques provides a promising tool for enhancing useful topological electrical responses relevant to future applications such as quantum information science [P. J. W. Moll, "Focused ion beam microstructuring of quantum matter," Annu. Rev. Condens. Matter Phys. 9, 147 (2018); Jang *et al.*, "Observation of half-height magnetization steps in Sr_2RuO_4," Science 331, 186 (2011); Moll *et al.*, "Transport evidence for Fermi-arc-mediated chirality transfer in the Dirac semimetal Cd_3As_2," Nature 535, 266 (2016); Moll *et al.*, "Evidence for hydrodynamic electron flow in $PdCoO_2$," Science 351, 1061 (2016)]. Here, we present microdevices fabricated with a focused ion beam from an indium-doped topological insulator $Pb_{1-x}Sn_xTe$. With the device thickness on the order of 1 μm and an extremely large bulk resistivity, we achieve an unprecedented enhancement of the surface contribution to about 30% of the total conductance near room temperature. The surface contribution increases as the temperature is reduced, becoming dominant below approximately 180 K, compared to 30 K in millimeter-thickness crystals. In addition to the enhanced surface contribution to normal-state transport, we observe the emergence of surface superconductivity below 6 K. Measurements of magnetoresistivity at high magnetic fields reveal a weak antilocalization behavior in the normal-state magnetoconductance at low temperatures and a variation in the power-law dependence of resistivity on temperature with the field. These results demonstrate that interesting electronic responses relevant to practical applications can be achieved by suitable engineering of single crystals.

Published under license by AIP Publishing. https://doi.org/10.1063/1.5122789

Tunable electrical responses and the emergence of superconductivity in topological insulators have garnered a broad interest in both academic and industrial communities due to their potential applications.[5,6] Three-dimensional topological crystalline insulators, with an inverted bulk bandgap and spin-momentum-locked metallic surface states protected by a crystalline symmetry, represent a useful quantum state of matter.[6–9] Theoretically, such topological crystalline insulators have been predicted for the rock salt crystal structure.[7,8,10] Subsequent photoemission spectroscopy measurements of $Pb_{1-x}Sn_xTe$ observed Dirac states near high-symmetry reciprocal lattice points.[11–14] $Pb_{1-x}Sn_xTe$ features a topological phase transition with doping x and hosts nontrivial surface states for x larger than ~0.35.[12,14] By compensating for defects with In substitution, the bulk resistivity of $Pb_{1-x}Sn_xTe$ can be unusually large for the intermediate x.[14,15] Surprisingly, a slightly higher In concentration can lead to the emergence of superconductivity.[16] As the resistivity of In-doped $Pb_{1-x}Sn_xTe$ is approximately two orders of magnitude greater than that of the most dilute superconductors (e.g., Ca-doped $SrTiO_3$),[15,17] the nature of superconductivity in $Pb_{1-x}Sn_xTe$ is at odds with the conventional Bardeen-Cooper-Schrieffer theory.[18]

Focused-ion-beam machining, which offers considerable flexibility in the precise control of the device geometry, has recently been applied to study topological materials, strongly correlated materials, and unconventional superconductors.[1–4] Geometric control of quantum devices has proved to be an effective method for manipulating surface and bulk responses.[3,14] In order to increase the surface-to-bulk response ratio and thus facilitate studies of surface electrical responses, we have fabricated microscale devices with an FEI Helios Nanolab 600 focused ion beam/scanning electron microscope DualBeam system. For clarity, in this letter, we only present detailed results on two devices, D1 ($84.0 \times 23.0 \times 0.5 \ \mu m^3$) and D2 ($75.0 \times 30.3 \times 1.8 \ \mu m^3$), fabricated from the same In-doped bulk crystal of $Pb_{1-x}Sn_xTe$ [$(Pb_{1-x}Sn_x)_{1-y}In_yTe$ with $x = 0.4$ and $y = 0.08$]. Similar behaviors are also observed for devices made on other topological materials, including $Pb_{1-x}Sn_xTe$ with other chemical concentrations. False-color scanning electron microscopy images of D1 and D2 are presented in Figs. 1(a) and 1(b), respectively. To minimize the surface damage, we polished the samples with the Ga^+ ion beam of selective energy and flux density (30 KeV/2.8 nA, 30 KeV/0.92 nA, 30 KeV/0.28 nA, 16 keV/0.47 nA,
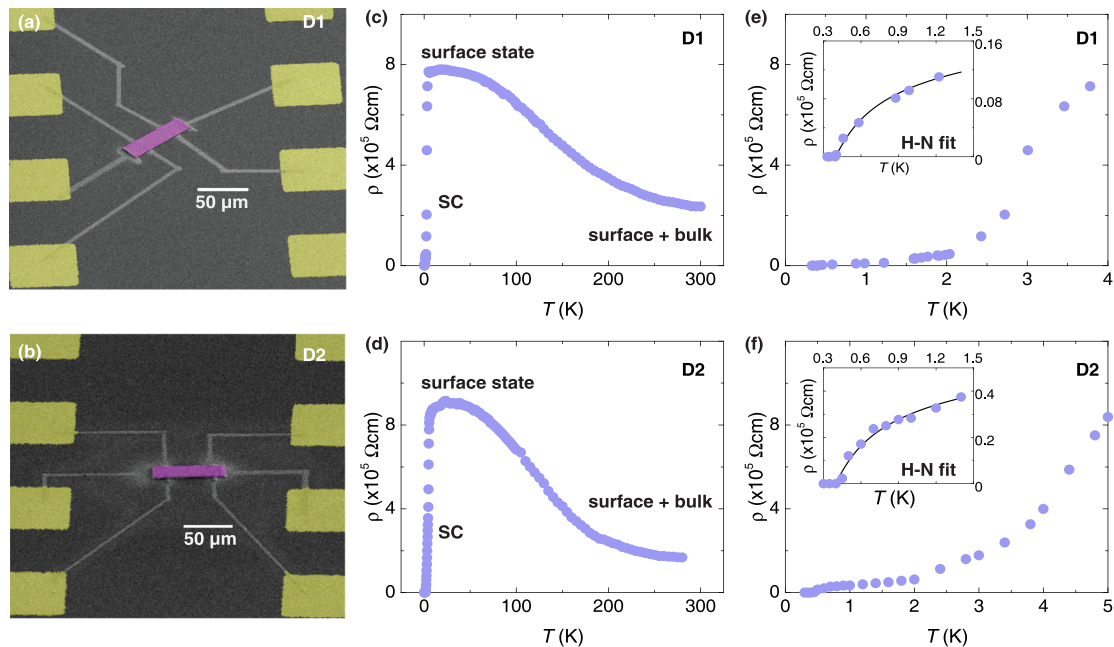
FIG. 1. $(Pb_{0.6}Sn_{0.4})_{0.92}In_{0.08}Te$ devices and possible two-dimensional superconductivity. (a) and (b) False-color scanning electron microscopy images of the crystals (purple), gold contacts (yellow), and platinum wires (gray) for D1 and D2, respectively. (c) and (d) Corresponding zero-field resistivity. (e) and (f) The emergence of possible two-dimensional superconductivity. For clarification, the insets show a fit to the Halperin-Nelson formula (H-N fit) up to 1.5 K [Eq. (1)].[19,20]

16 keV/45 pA, and 8 keV/11 pA in a consecutive order) before an *in situ* lift-out procedure using a micromanipulator probe. The lift-out samples were placed on SiO_2/Si (300 nm SiO_2 thickness) wafers with gold pads prefabricated using optical lithography and electron-beam physical vapor deposition (Kurt J. Lesker PVD 75 E-beam evaporator). *In situ* electron-beam-assisted deposition of platinum was used to connect samples with gold pads and the fabricated devices were annealed at 120 °C for 20 min to ensure Ohmic contacts. Both D1 and D2 were made such that their edges are along equivalent crystalline *a* axes. Energy-dispersive X-ray spectroscopy (EDS) measurements were performed on D1 and pristine In-doped $Pb_{1-x}Sn_xTe$ crystals using an analytical scanning electron microscope JEOL 7600F. The variations among the atomic weights of Pb, Sn, and Te are within 4%, suggesting that the alteration of the $Pb_{1-x}Sn_xTe$ structure is minimal during the device fabrication. The Ga concentration for D1 is observed to be 0.08 ± 0.02.

The zero-field electrical resistivity of D1 and D2 was measured down to 0.3 K using an Oxford 3He vacuum insert system and a Janis CPX-HF micromanipulator probe station [Figs. 1(c) and 1(d), respectively]. Both devices are very good insulators with the resistivity around $8 \times 10^5 \Omega$ cm at 10 K, indicating a negligible doping effect from Ga ions in the bulk. At the same time, the drop in resistivity below 6 K suggests the emergence of superconducting fluctuations, a state that is not present in the parent crystal.[14,16] As shown in Figs. 1(e) and 1(f), the resistivity only reaches zero below 0.4 K. The strongly reduced but finite resistivity below 2 K is consistent with the presence of two-dimensional (2D) superconducting fluctuations above the phase-ordering temperature. The lines through the data points in the insets of Figs. 1(e) and 1(f) represent the fits to the Halperin-Nelson formula for the resistivity of a phase-fluctuating 2D superconductor[19,20]

$$\rho(T) = \rho e^{-b/\sqrt{T/T_{BKT}-1}}, \qquad (1)$$

where T_{BKT} is the Berezinskii-Kosterlitz-Thouless transition temperature[21,22] at which resistivity becomes zero. ρ and b are the other fit parameters. The fits yield $T_{BKT} = 0.36$ K, $\rho = 2.98 \times 10^4 \Omega$ cm, and $b = 1.4$ for D1 and $T_{BKT} = 0.38$ K, $\rho = 7.74 \times 10^4 \Omega$ cm, and $b = 1.2$ for D2. The similarities in T_{BKT} and b indicate a consistent behavior in both devices.

To interpret the possible source of superconductivity, it is relevant to know that while $(Pb_{0.6}Sn_{0.4})_{1-y}In_yTe$ is a bulk insulator for y = 0.08, it is a bulk superconductor for y = 0.2 and 0.3 with $T_c \sim 4$ K.[16] Ga is chemically similar to In and found to be present at the surface with a concentration similar to In, which raises the possibility that doping by Ga in the near-surface region has induced the superconductivity. To check this possibility, we added 10% Ga to an insulating bulk $(Pb_{0.6}Sn_{0.4})_{1-y}In_yTe$ crystal with y = 0.1, melted the combination, and allowed it to solidify. The resulting material exhibited a diamagnetic response with a volume shielding fraction between 10% and 50% and an onset temperature for superconductivity as high as 7.3 K. While additional work is required to identify the exact superconducting phase and we cannot rule out a possibility of modifications in the electronic structure due to the surface strain of the microdevices induced by focused ion beam fabrication,[23] the added Ga seems to be responsible for the surface superconductivity in our devices. If the coherence length [~12 nm for $(Pb_{0.5}Sn_{0.5})_{0.84}In_{0.16}Te$, Ref. 14] is smaller than the layer thickness, then the superconductivity should have a 2D character. Based on the ion beam energy used and the hardness of $Pb_{1-x}Sn_xTe$ materials,[1] we qualitatively estimate the penetration depth to be on the order of 10 nm. The net effect, obtaining a superconducting layer at the surface of a topological bulk phase, is similar to that achieved by selective ion sputtering on NbAs.[24]
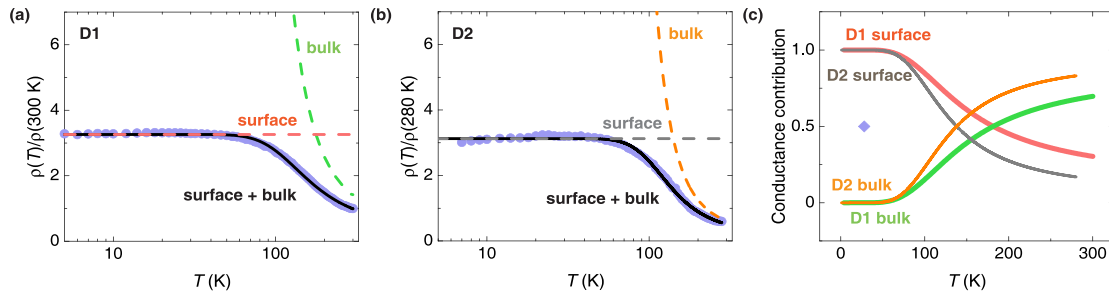
FIG. 2. Surface and bulk contributions. (a) and (b) Temperature dependence of the normalized resistivity ratio for D1 and D2, respectively. The solid lines denote a fit to the parallel conductance equation [Eq. (2)]. The dashed line presents the surface and bulk resistivity. (c) Temperature dependences of the surface and bulk conductance contributions. The blue Diamond indicates $T_h \approx 30$ K for the bulk crystals.[14] $T_h = 182$ K for D1 and 137 K for D2.

Next, we consider the insulating behavior in the normal state. The temperature dependence of resistivity is very useful for distinguishing the surface and bulk contributions. Assuming that the surface and bulk states contribute to the conduction channels in parallel, the normalized resistivity ratio, $r(T) \equiv \rho(T)/\rho(T_0)$, can be expressed as[14,25,26]

$$1/r(T) = 1/r_s + 1/r_b e^{-\Delta/k_B T}, \qquad (2)$$

where $T_0 = 300$ K for D1 and 280 K for D2. $1/r_s$ denotes the surface conduction assumed to be temperature independent,[14,25,26] and $1/r_b e^{-\Delta/k_B T}$ denotes the thermally activated bulk conductance. The fitted results are shown in Fig. 2, with the corresponding parameters $r_s = 3.26$, $r_b = 0.39$, and $\Delta = 32.4$ meV for D1 and $r_s = 5.27$, $r_b = 0.24$, and $\Delta = 36.7$ meV for D2. The similarities of r_b and Δ indicate a consistent bulk response in the two devices. The fraction of surface and bulk contributions to the total conductance can be evaluated as $r(T)/r_s$ and $r(T)/r_b$, respectively. In Fig. 2(c), we compare the conductance contributions. The temperature at which the surface states constitute half of the total conductance (T_h) is found to be approximately 30 K for samples with thicknesses between 0.20 and 0.60 mm.[14] The relatively small surface contribution and the low T_h limits the sensitivity to the surface state. For D1 and D2, which have a device thickness of 0.5 μm and 1.8 μm, respectively, the T_h is enhanced to 182 K and 137 K. The relative surface contributions near room temperature are 30% and 19%, respectively.

The impact of the magnetic field on the resistivity of D1 was probed using the 35 T resistive magnet and a 3He cryostat at the DC Field Facility, National High Magnetic Field Laboratory. The measurements were performed with Signal Recovery 7265 lock-in amplifiers and Lake Shore 372 AC resistance bridge systems. The raw magnetoresistivity results are plotted in Fig. 3(a). The normalized magnetoresistivity, $\Delta\rho/\rho_0$, where $\Delta\rho \equiv \rho(\mu_0 H) - \rho_0$, is shown in Fig. 3(b). Weak oscillations are found at 0.48 K, but they are already undetectable at 0.58 K. Above 6 K, the electrical resistivity of D1 is finite for the entire field range and we define $\rho_0 \equiv \rho(\mu_0 H = 0$ T$)$. Below 6 K, superconductivity exists at a low magnetic field and ρ_0 is obtained by extrapolating the high magnetic field ($\mu_0 H \geq 10$ T) resistivity to zero field, using the form $\rho(\mu_0 H) = \rho_0 + aH^n$. Remarkably, the high-magnetic-field dependence of $\rho(\mu_0 H)$ is described by $n \approx 1$ below 2 K. This field dependence was previously reported in other topological insulator thin films,[27,28] and it was associated with

the topological surface states. n gradually increases to 1.7 at 20 K, above which it saturates, as shown in Fig. 3(c). Correspondingly, $\Delta\rho(\mu_0 H = 35$ T$)/\rho_0$, a measure of the fractional change in magnetoresistivity, decreases dramatically with temperature.

To further analyze the surface contribution, we convert the magnetoresistivity into magnetoconductance. The magnetoconductance of topological crystalline insulators has been associated with the quantum interference between scattering trajectories of surface states.[5–9] With a π Berry phase, destructive quantum interference suppresses back scattering. This destructive quantum interference can be destroyed by applying external magnetic fields, leading to a decrease in the magnetoconductance.[14,29] Magnetoconductance near the superconducting transition temperature is plotted in Fig. 3(d), which can be described by the weak antilocalization behavior using the Hikami-Larkin-Nagaoka equation[29]
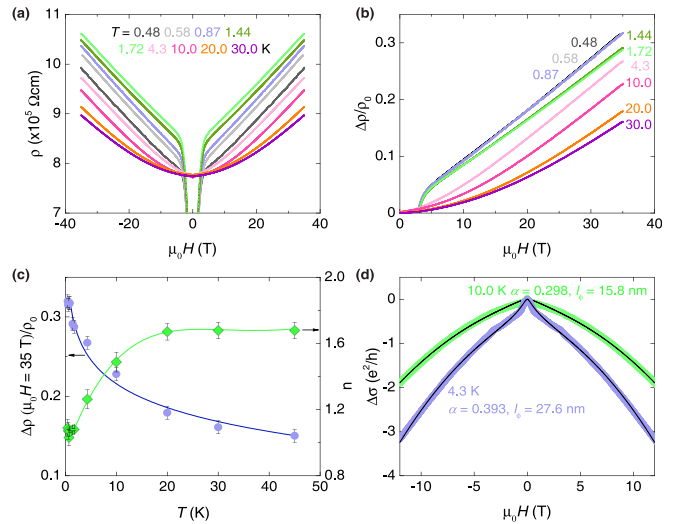

FIG. 3. High-magnetic-field electrical responses for D1. (a) Magnetoresistivity data at various temperatures. (b) Normalized magnetoresistivity showing a variation in the power-law dependence of resistivity on temperature with the field. (c) Temperature dependences of $\rho(35$ T$)/\rho_0$ and power index n. (d) Magnetoconductance and fits to the Hikami-Larkin-Nagaoka equation [Eq. (3)], showing a weak antilocalization behavior.[14,29]

$$\Delta\sigma = \alpha \frac{e^2}{\pi h}\left[\ln\left(H_\phi/H\right) - \psi\left(H_\phi/H + 1/2\right)\right], \qquad (3)$$

where ψ is the digamma function and H_ϕ is the phase-coherence characteristic field. For indium-doped $Pb_{1-x}Sn_xTe$, the Fermi surface crosses four Dirac cones and α is predicted to be close to 2. The fits to 4.3 and 10 K data yield $\alpha = 1.23$, $l_\phi = 27.6$ nm and $\alpha = 0.94$, $l_\phi = 15.8$ nm, respectively. $l_\phi = \sqrt{\hbar/4eH_\phi}$ denotes the electron coherence length, which exhibits a slight reduction as the thermal fluctuations increase, consistent with the previously reported results.[14]

In summary, we report an unprecedented enhancement of surface conductance for $Pb_{1-x}Sn_xTe$ devices using microstructuring techniques. The temperature T_h at which surface states constitute half of the total conductance is increased to about 180 K and a 30% surface contribution is observed near room temperature. Furthermore, we observe an approximately linear magnetoresistivity and the emergence of surface superconductivity with a 2D character at low temperatures. These electrical responses, likely related to an enhanced surface conductance, point to a useful engineering of single crystals toward potential applications.

See the supplementary material for the diamagnetic response of the melt $(Pb_{0.6}Sn_{0.4})_{0.9}In_{0.1}Te$ crystal added with Ga and the representative EDS results for D1.

REFERENCES

[1]P. J. W. Moll, "Focused ion beam microstructuring of quantum matter," Annu. Rev. Condens. Matter Phys. **9**, 147 (2018).

[2]J. Jang, D. G. Ferguson, V. Vakaryuk, R. Budakian, S. B. Chung, P. M. Goldbart, and Y. Maeno, "Observation of half-height magnetization steps in Sr_2RuO_4," Science **331**, 186 (2011).

[3]P. J. W. Moll, N. L. Nair, T. Helm, A. C. Potter, I. Kimchi, A. Vishwanath, and J. G. Analytis, "Transport evidence for Fermi-arc-mediated chirality transfer in the Dirac semimetal Cd_3As_2," Nature **535**, 266 (2016).

[4]P. J. W. Moll, P. Kushwaha, N. Nandi, B. Schmidt, and A. P. Mackenzie, "Evidence for hydrodynamic electron flow in $PdCoO_2$," Science **351**, 1061 (2016).

[5]J. Wang and S. C. Zhang, "Topological states of condensed matter," Nat. Mater. **16**, 1062 (2017).

[6]M. Z. Hasan, S. Xu, and G. Bian, "Topological insulators, topological superconductors and Weyl fermion semimetals: Discoveries, perspectives and outlooks," Phys. Scr. **T164**, 014001 (2015).

[7]L. Fu, "Topological crystalline insulators," Phys. Rev. Lett. **106**, 106802 (2011).

[8]X.-L. Qi and S.-C. Zhang, "Topological insulators and superconductors," Rev. Mod. Phys. **83**, 1057 (2011).

[9]Y. Ando and L. Fu, "Topological crystalline insulators and topological superconductors: From concepts to materials," Annu. Rev. Condens. Matter Phys. **6**, 361 (2015).

[10]T. H. Hsieh, H. Lin, J. Liu, W. Duan, A. Bansil, and L. Fu, "Topological crystalline insulators in the SnTe material class," Nat. Commun. **3**, 982 (2012).

[11]P. Dziawa, B. J. Kowalski, K. Dybko, R. Buczko, A. Szczerbakow, M. Szot, E. Łusakowska, T. Balasubramanian, B. M. Wojek, M. H. Berntsen, O. Tjernberg, and T. Story, "Topological crystalline insulator states in $Pb_{1-x}Sn_xSe$," Nat. Mater. **11**, 1023 (2012).

[12]S.-Y. Xu, C. Liu, N. Alidoust, M. Neupane, D. Qian, I. Belopolski, J. D. Denlinger, Y. J. Wang, H. Lin, L. A. Wray, G. Landolt, B. Slomski, J. H. Dil, A. Marcinkova, E. Morosan, Q. Gibson, R. Sankar, F. C. Chou, R. J. Cava, A. Bansil, and M. Z. Hasan, "Observation of a topological crystalline insulator phase and topological phase transition in $Pb_{1-x}Sn_xSe$," Nat. Commun. **3**, 1192 (2012).

[13]C. Yan, J. Liu, Y. Zang, J. Wang, Z. Wang, P. Wang, Z.-D. Zhang, L. Wang, X. Ma, S. Ji, K. He, L. Fu, W. Duan, Q.-K. Xue, and X. Chen, "Experimental observation of Dirac-like surface states and topological phase transition in $Pb_{1-x}Sn_xSe$ (111) films," Phys. Rev. Lett. **112**, 186801 (2014).

[14]R. Zhong, X. He, J. A. Schneeloch, C. Zhang, T. Liu, I. Pletikosić, T. Yilmaz, B. Sinkovic, L. Qiang, W. Ku, T. Valla, J. M. Tranquada, and G. D. Gu, "Surface-state-dominated transport in crystals of the topological crystalline insulator In-doped $Pb_{1-x}Sn_xTe$," Phys. Rev. B **91**, 195321 (2015).

[15]K. Ran, R. Zhong, T. Chen, Y. Gan, J. Wang, B. L. Winn, A. D. Christianson, S. Li, Z. Ma, S. Bao, Z. Cai, G. Xu, J. M. Tranquada, G. D. Gu, J. Sun, and J. Wen, "Unusual phonon density of states and response to the superconducting transition in the In-doped topological crystalline insulator $Pb_{0.5}Sn_{0.5}Te$," Phys. Rev. B **97**, 220502(R) (2018).

[16]R. Zhong, J. Schneeloch, Q. Li, W. Ku, J. M. Tranquada, and G. D. Gu, "Indium substitution effect on the topological crystalline insulator family $(Pb_{1-x}Sn_x)_{1-y}In_yTe$: Topological and superconducting properties," Crystals **7**, 55 (2017).

[17]X. Lin, Z. Zhu, B. Fauqué, and K. Behnia, "Fermi surface of the most dilute superconductor," Phys. Rev. X **3**, 021002 (2013).

[18]J. Bardeen, L. N. Cooper, and J. R. Schrieffer, "Theory of superconductivity," Phys. Rev. **108**, 1175 (1957).

[19]Q. Li, M. Hücker, G. D. Gu, A. M. Tsvelik, and J. M. Tranquada, "Two-dimensional superconducting fluctuations in stripe-ordered $La_{1.875}Ba_{0.125}CuO_4$," Phys. Rev. Lett. **99**, 067001 (2007).

[20]B. I. Halperin and D. R. Nelson, "Resistive transition in superconducting films," J. Low Temp. Phys. **36**, 599 (1979).

[21]V. L. Berezinskii, "Destruction of long-range order in one-dimensional and two-dimensional systems possessing a continuous symmetry group. II. Quantum systems," Zh. Eksp. Teor. Fiz. **61**, 1144 (1971) [Sov. Phys. JETP **34**, 610 (1972)], available at http://www.jetp.ac.ru/cgi-bin/e/index/e/34/3/p610?a=list.

[22]J. M. Kosterlitz and D. J. Thouless, "Ordering, metastability and phase transitions in two-dimensional systems," J. Phys. C **6**, 1181 (1973).

[23]F. Hofmann, E. Tarleton, R. J. Harder, N. W. Phillips, P. Ma, J. N. Clark, I. K. Robinson, B. Abbey, W. Liu, and C. E. Beck, "3D lattice distortions and defect structures in ion-implanted nano-crystals," Sci. Rep. **7**, 45993 (2017).

[24]M. D. Bachmann, N. Nair, F. Flicker, R. Ilan, T. Meng, N. J. Ghimire, E. D. Bauer, F. Ronning, J. G. Analytis, and P. J. W. Moll1, "Inducing superconductivity in Weyl semimetal microstructures by selective ion sputtering," Sci. Adv. **3**, e1602983 (2017).

[25]A. A. Taskin, Z. Ren, S. Sasaki, K. Segawa, and Y. Ando, "Observation of Dirac holes and electrons in a topological insulator," Phys. Rev. Lett. **107**, 016801 (2011).

[26]D.-J. Kim, J. Xia, and Z. Fisk, "Topological surface state in the Kondo insulator samarium hexaboride," Nat. Mater. **13**, 466 (2014).

[27]H. He, B. Li, H. Liu, X. Guo, Z. Wang, M. Xie, and J. Wang, "High-field linear magneto-resistance in topological insulator Bi_2Se_3 thin films," Appl. Phys. Lett. **100**, 032105 (2012).

[28]B. A. Assaf, T. Cardinal, P. Wei, F. Katmis, J. S. Moodera, and D. Heiman, "Linear magnetoresistance in topological insulator thin films: Quantum phase coherence effects at high temperatures," Appl. Phys. Lett. **102**, 012102 (2013).

[29]S. Hikami, A. I. Larkin, and Y. Nagaoka, "Spin-orbit interaction and magneto-resistance in the two dimensional random system," Prog. Theor. Phys. **63**, 707 (1980).